PCCP

PAPER

The Effect of Mg^{2+} Incorporation on the Structure of Calcium Carbonate Clusters: Investigation by the Anharmonic Downward Distortion Following Method

Received 00th January 20xx,
Accepted 00th January 20xx

DOI: 10.1039/x0xx00000x

www.rsc.org/

Jun Kawano,[a,b] Satoshi Maeda,[c] and Takaya Nagai[b]

Mg^{2+} is considered to play an important role in the formation of calcium carbonate polymorphs; however, how it affects polymorph selection during the early stages of $CaCO_3$ formation is not yet well understood. In the present study, in order to clarify the effect of Mg^{2+} on the nucleation of calcium carbonate polymorphs, the stable structures of anhydrous additive-free and Mg-containing calcium carbonate clusters are derived using the anharmonic downward distortion following method, based on quantum chemical calculation. Optimization is performed at the B3LYP/6-31+G(d) level and the solvent effect is induced by the self-consistent reaction field method using the conductor-like polarized continuum calculation model. Calculation results show that incorporating Mg^{2+} into clusters can change the clusters' stable configuration. In case of dimers and trimers, a Mg ion strongly prefers to locate at the centre of the clusters, which suggests that Mg is easy to incorporate into the clusters once it is released from its tight hydration shell. Notably, structures similar to the crystalline phase appear when only four $CaCO_3$ units aggregate into the cluster: in the stable structure of the additive-free $CaCO_3$ tetramer, the arrangement of Ca and CO_3 ions is almost the same as that of the calcite structure, while the structure of the Mg-containing $CaCO_3$ tetramer resembles the aragonite structure in the way that CO_3 ions are stacked. These results indicate that Mg can play a key role in aragonite formation not only by inhibiting calcite growth but also by directly promoting aragonite nucleation in the early stages of $CaCO_3$ formation.

1. Introduction

Calcium carbonate ($CaCO_3$) occurs in six different forms: three crystalline polymorphs (calcite, aragonite and vaterite), two hydrate phases (monohydrocalcite and ikaite) and amorphous calcium carbonate (ACC). At room temperature and pressure, calcite is thermodynamically stable and expected to form predominantly. However, exceptions to this rule are widely known—for instance, shellfish shells and coral skeletons consist dominantly of aragonite, which is the high pressure phase of $CaCO_3$. Apart from these examples, most organisms form tissues with various polymorphs. The ability to select and use these polymorphs for their own functional requirements is fundamental to these organisms' lives; thus, the occurrence of $CaCO_3$ in living organisms has received considerable attention[1] and the formation conditions and mechanisms of different polymorphs are important. In order to understand this kind of biogenetic $CaCO_3$ formation, it is necessary to understand the physical principles of the inorganic formation of calcium carbonate polymorphs; yet, our knowledge of the $CaCO_3$ formation process—especially that concerning polymorph selection—is far from complete.

The formation process of $CaCO_3$ polymorphs from aqueous solutions has attracted research for more than a century[2–6]; consequently, a large number of controlling phenomena have been put forward as accounting for the formation of any given polymorph. In particular, Mg^{2+} has been considered important for the formation of $CaCO_3$ polymorphs, and Kitano [3] pointed out that addition of Mg^{2+} into a solution promotes the metastable formation of aragonite. In general, divalent cations smaller than Ca^{2+}, such as Mg^{2+}, do not enter the aragonite structure, and all Mg-containing carbonate minerals (e.g. high-Mg calcite, dolomite $CaMg(CO_3)_2$ and magnesite $MgCO_3$) have a calcite structure and not an aragonite structure; therefore, this phenomenon seems paradoxical. Yet, recent observations of the growth surface of calcite (using the atomic force microscope (AFM)) have revealed that Mg^{2+} inhibits calcite crystal growth by blocking propagation of the kink[7] or increasing mineral solubility[8], which leads to aragonite formation. Although its effect on nucleation is not fully understood, it is important because polymorph selection is determined during nucleation. Thus, we focus on the effect of Mg^{2+} on early-stage $CaCO_3$ formation.

Unlike the traditional nucleation theory, a crystallization pathway through non-classical mechanisms has recently been

[a] Creative Research Institution (CRIS), Hokkaido University. N21 W10 Kita-ku, Sapporo, Hokkaido, 001-0021 Japan
[b] Department of Earth and Planetary Sciences, Faculty of Science, Hokkaido University, N10 W8 Kita-ku, Sapporo, Hokkaido, 060-0810 Japan .
[c] Department of Chemistry, Faculty of Science, Hokkaido University, N10 W8 Kita-ku, Sapporo, Hokkaido, 060-0810 Japan

put forward as a possible method for early-stage $CaCO_3$ formation[9–12]. Using ion potential measurements in combination with analytical ultracentrifugation, Gebauer et al. have proposed the existence of stable prenucleation clusters of $CaCO_3$[9]. Later, Pouget et al. used a cryogenic transmission electron microscope to directly observe and confirm the existence of those same clusters[13]. There have also been many attempts to use computer simulation to understand early-stage $CaCO_3$ formation[14–19]. For example, Raiteri and Gale used a molecular dynamics (MD) simulation with a newly developed accurate force field to show that the free energy of amorphous calcium carbonate (ACC) should decrease as more ion pairs of calcium carbonate form from the solution, suggesting that initial formation of $CaCO_3$ may be barrierless and non-classical[15]. Furthermore, Demichelis et al. have expanded Raiteri and Gale's technique to bicarbonate ions and shown that prenucleation clusters are liquid-like ionic polymers[18].

These recent works provide a new picture of how early-stage calcium carbonate growth occurs; however, how this non-classical pathway affects polymorph selection and what kind of role Mg does play in the context of such a prenucleation pathway is still under debate. Recently, Kawano et al.[20] performed a first-principles study of a Mg-containing aragonite surface and indicated that Mg^{2+} substituted into a Ca site near the surface changes the surface structure. Moreover, Mg^{2+} ions strongly prefer six-coordinate geometry. Thus, the presence of Mg^{2+} affects the surface stability of aragonite and may affect the structure of small clusters appearing during early $CaCO_3$ formation, where ions are even easier to move than on the surface, both of which affect the polymorph selection of $CaCO_3$.

As far as understanding early-stage $CaCO_3$ formation in aqueous solutions, the MD simulations mentioned above[15, 18] actually achieved remarkable results; however, this technique cannot be adopted to systems including Mg^{2+} because a Mg^{2+} ion in aqueous solutions forms a tight hydration shell with water molecules from which it cannot be released within the time scale of computer simulations. Therefore, in the present study, we use the anharmonic downward distortion following (ADDF) method[21-24] to make quantum chemical calculations intended to investigate the stable structure of Mg-containing calcium carbonate clusters. The ADDF method was recently developed to make an automated global exploration for reaction pathways on the quantum chemical potential energy surface (PES) of a given chemical formula possible without any assumptions of initial structures and reaction routes. In many cases, this method has been found to produce successful applications for the chemical reaction of molecules[24–28]. Furthermore, in such a case as this, where the structure of clusters is completely unknown, ADDF should be highly suitable in searching for stable configurations; however, it should be noted that there is no precedent for applying this technique to the early stages of crystal formation.

Many previous calculations regarding early-stage $CaCO_3$ formation have shown that water plays an important role in the formation of ACC and prenucleation clusters[15,18]; however, Roass-García et al. analysed the stable configurations of neutral gas phase clusters of $(CaCO_3)_n$ (n = 2–7) and concluded that the stable structures of those clusters resemble neither calcite nor aragonite and that ACC is not caused by the solvent effect[19]. Because calculations explicitly including many water molecules are currently too expensive for use with the ADDF method, the present study uses the self-consistent reaction field (SCRF) method as a first step to inducing the solvent effect, which means that calculation in the presence of a solvent is conducted by placing the solute in a cavity within the solvent reaction field[29]. Therefore, the present calculations can be considered to simulate the onset of the first anhydrous phase.

With this background, the aims of the present study are to (1) verify the usefulness of ADDF when investigating early-stage $CaCO_3$ formation and (2) clarify the effect of Mg^{2+} incorporation on the nucleation of calcium carbonate polymorphs by deriving the stable and transition structures of anhydrous additive-free and Mg-containing $CaCO_3$ clusters.

2. Calculation Methods

The ADDF method implemented in the GRRM program was used in combination with the Gaussian09 package[30]. To find equilibrium structures (EQs) and transition structures (TSs) and to achieve a global reaction route map, both uphill walking and downhill walking along the reaction pathway are necessary. Downhill walking from the TS to the EQ along the minimum energy path can be made by conventional methods, such as steepest descent approach; however, uphill walking along a reaction route from the EQ towards the TS has long been a major challenge since an efficient search of the initial directions of reaction routes starting from the EQ have previously been impossible. The ADDF method overcomes this problem with the search of reaction paths by following an anharmonic downward distortion (ADD)[21]. Along the reactive potential curves, the potential changes from concave to convex. In other words, an ADD, i.e. energy lowering from the second-order (harmonic) potential owing to third and higher-order (anharmonic) terms, occurs along these potential curves. Therefore, this method employs a simple principle: reaction paths can be found in maximal ADD directions. Furthermore, another principle, i.e. a larger ADD leads to a lower TS and a lower product, can naturally be expected. Thus, the large-ADD (l-ADD) technique is available for fast searches in ADDF, which is expected to explore the low energy structures along low barrier pathways[31]; it has been successfully applied to various systems[27,28,31] and is applied also in the present study. The methods used to efficiently find maximal ADD directions in multi-dimensional potential-energy surfaces and the methods used to effectively choose l-ADDs from various ADDs have been described in previous papers[21-24,31].

A detailed description of our study's method is as follows.

1. Start with three or four structures in which Ca and CO_3 are randomly arranged.
2. Roughly search the equilibrium and transition structures at the B3LYP/6-31G level with following five *l*-ADDs around each EQ.

3. Perform structure refinement of each EQ and TS at the B3LYP/6-31+G(d) level. SCRF calculations are performed by the conductor-like polarized continuum model (CPCM)[32].

We performed normal mode analysis for all obtained structures to confirm whether each structure had one or more imaginary frequencies. In addition, starting from all obtained first-order saddle points, we computed the intrinsic reaction coordinate (IRC) to identify the path connectivity. This technique has been applied to additive-free calcium carbonate clusters, $(CaCO_3)_n$ (n = 2–4) and Mg-containing clusters in which one Mg ion is substituted for Ca, $Ca_nMg(CO_3)_{n+1}$ (n = 1–3). For comparison, the energies of $CaCO_3$ and $MgCO_3$ ion pairs (monomers) were calculated to be −941.561061 and −464.038783 Hartree, respectively. The atomic arrangements of the clusters were illustrated using Chemcraft software, unless otherwise noted.

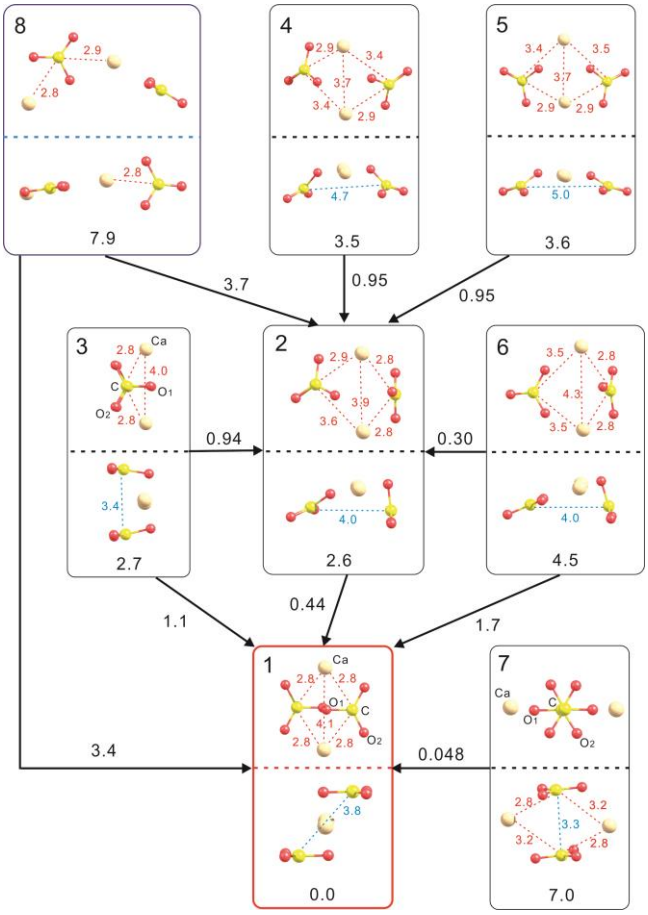

Fig. 1. Equilibrium structures of an additive-free dimer $(CaCO_3)_2$ and the connections between them. Each equilibrium structure, which is illustrated from two directions, is labelled in order of stability (with Structure **1** being the most stable). Underneath each structure, the relative energy (based on that of the most stable structure) is shown in kcal/mol. Numbers with an arrow represent the activation energy necessary for structural change when that change proceeds in the direction shown by the arrow. In each image, white circles represent Ca, red circles O and yellow C. Dotted lines and their subscripts represent the interatomic distance in Å.

3. Results and Discussion

3.1 Equilibrium structures of $CaCO_3$ dimers and trimers

When a $CaCO_3$ dimer forms without Mg^{2+}, several configurations appear as stable structures; these are divided into eight types. Equilibrium structures, along with their relative energy (based on the energy required by the most stable structure), are illustrated in Fig. 1. In this figure, the most stable arrangement is shown as Structure **1**, which is also reported in the previous calculation as the most stable configuration of a dimer in a gas phase[19]. Some structures appear in both the present and previous calculations while others are observed in only one or the other. Use of the SCRF method to recreate the solvent effect or use of different calculation levels (Hartree-Fock (HF) in previous calculations and the density functional theory (DFT) in the present study) may account for such differences. The relative energies of the dimers obtained in this study are much lower than those obtained by previous HF calculations. It should be noted that the relationship of the magnitudes of the relative energies of these equilibrium structures does not change with or without the zero-point energy correction.

Table. 1 Equilibrium structures and energies obtained at various calculation levels

Structure 1

Functional	Basis set	ΔE	Ca-Ca	C-C	C-O_1	C-O_2
B3LYP	6-31+G(d)	0	4.145	3.775	1.320	1.290
M062X	6-32+G(d)	0	4.123	3.646	1.313	1.283
wB97XD	6-33+G(d)	0	4.173	3.717	1.311	1.285
B3LYP	6-311+G(2d)	0	3.964	3.662	1.319	1.281
		(kcal/mol)				(Å)

Structure 3

Functional	Basis set	ΔE	Ca-Ca	C-C	C-O_1	C-O_2
B3LYP	6-31+G(d)	2.674	4.054	3.348	1.322	1.290
M062X	6-32+G(d)	2.780	3.985	3.206	1.315	1.282
wB97XD	6-33+G(d)	2.333	4.058	3.326	1.313	1.283
B3LYP	6-311+G(2d)	2.599	3.851	3.256	1.321	1.280
		(kcal/mol)				(Å)

Structure 7

Functional	Basis set	ΔE	Ca-Ca	C-C	C-O_1	C-O_2
B3LYP	6-31+G(d)	7.018	5.015	3.253	1.297	1.301
M062X	6-32+G(d)	8.927	5.093	3.051	1.290	1.293
wB97XD	6-33+G(d)	6.651	5.091	3.193	1.291	1.294
B3LYP	6-311+G(2d)	6.509	4.860	3.131	1.291	1.294
		(kcal/mol)				(Å)

*Refer to Fig. 1 for structure numbers and atomic arrangements.

In the present study, we explored the equilibrium and transition structures at the B3LYP/6-31+G(d) level. In order to justify this choice, the optimizations of the equilibrium structures were performed with different functionals and basis sets around these structures. Table 1 shows the optimized structures and the energies calculated at the B3LYP/6-31+G(d), M062X/6-31+G(d), wB9797XD/6-31+G(d) and B3LYP/6-311+G(2d) levels, which demonstrates that the equilibrium derived at the B3LYP/6-31+G(d) level is also at equilibrium at the other calculation levels. In addition, the magnitude correlation is the same among all calculations at various levels. Therefore, the B3LYP/6-31+G(d) level is considered to be accurate enough for the present purpose. Furthermore, Table 1 shows that in most cases, the symmetry of the CO_3^{2-} does not retain D_{3h}, which indicates the possibility that the measurements of the vibrational spectra provides evidence for the success of these models when comparing the calculation results of the frequencies of these clusters in a manner similar to that in recent studies[33,34]. However, because there are various structures in this system including both crystalline and amorphous phases[35], it is difficult to correctly assign the difference among the frequencies of these structures in aqueous solutions at this stage. This should be an interesting future topic.

The ADDF method can explore transition structures when one equilibrium structure transfers to another. This leads to specification of the reaction route, and the activation energy of that route can be obtained as the energy of the transition state. Fig. 1 shows both the reaction routes between two equilibrium structures and the activation energies which is related to the reaction rate, required for those paths; the global route mapping is established. Structure **8**, which has the most energy of all the equilibrium structures, shows a direct connection of two $CaCO_3$ ion pairs; thus, it would be relatively easy to form

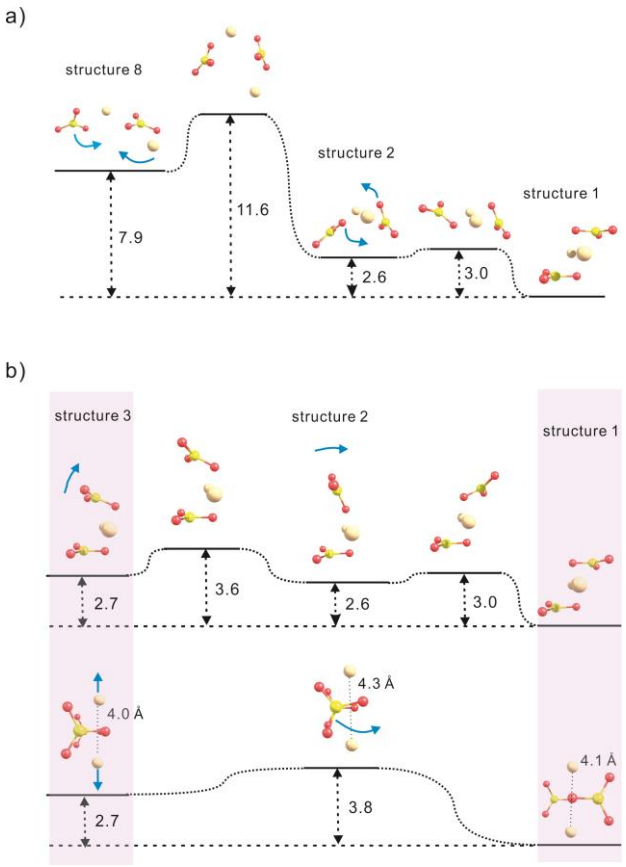

Fig. 2. Examples of the structural change process in additive-free $CaCO_3$ dimers. (a) Reaction path between Structure **8**, which requires the most energy and Structure **1**. (b) Reaction paths between Structures **3** and **1**. Two types of reaction paths are shown: where the CO_3 ion 'overhangs' (above) and where CO_3 slides to another position (bottom). These two paths require almost the same activation energy. The relative energy of each equilibrium or transition structure based on the most stable structure is also shown in kcal/mol.

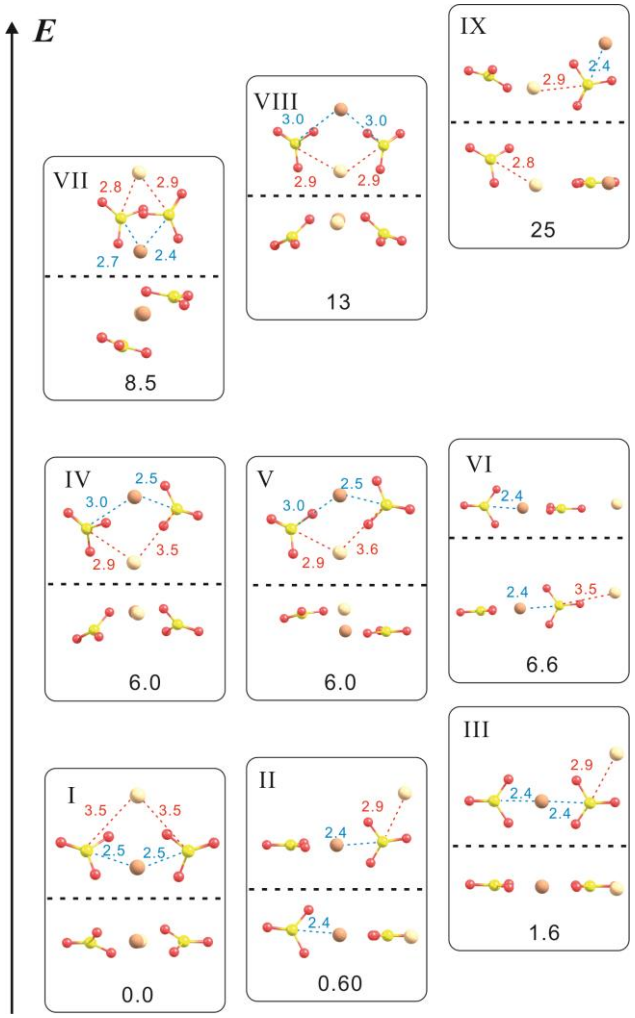

Fig. 3. Equilibrium structures of Mg-containing dimers, $CaMg(CO_3)_2$. Orange circles represent Mg; other expressions are the same as in Fig. 1. Dotted lines and their supscripts represent the interatomic distance in Å.

Structure **8** from separate $CaCO_3$ monomers. Fig. 1 shows the routes that structurally change the least stable Structure **8** into the most stable Structure **1** and suggests that there are several paths for achieving the most stable condition. Fig. 2 illustrates examples of structural change routes and clearly shows the atomic behaviour of the stable cluster's generation process, further indicating ADDF's usefulness.

The structures of Mg-containing dimers, $CaMg(CO_3)_2$, are significantly different from those of additive-free $CaCO_3$ dimers. Exploration with ADDF identifies nine distinct structures (shown in Fig. 3). In each arrangement, small structural changes, including the tilt or rotation of CO_3 groups, are allowed without significant energetic change. That figure shows that configurations in which a Mg ion is located between two CO_3 groups (Structures **I–III**) have the lowest energies. In contrast, structures in which Mg ions are arranged outside the cluster (Structures **VIII** and **IX**) have much higher energy. The difference in energy between the two types of clusters is much larger than in the case of pure $CaCO_3$ dimers, which suggests that a Mg ion strongly prefers to locate at the centre of clusters. Note that, in Structure **VI**, a Ca ion is desorbed from the cluster and then easily absorbed back in without the energy barrier; the stable configuration (Structure **I**) is then achieved.

In additive-free trimers, $(CaCO_3)_3$, which have the lowest energy, Ca ions are located in positions that then become the apexes for equilateral triangles that are about 4.7 Å on a side. CO_3^{2-} groups can be configured in one of two ways: (1) across the plane formed by three Ca^{2+} ions, two CO_3 groups can be arranged on one side while the other CO_3 is located on another side (Structure **9**) or (2) all three CO_3 groups are arranged on the same side against the plane (Structure **10**) and serve as the three hold rotation axes at the centre of the triangle formed by Ca ions (Fig. 4). The former type of structure has a relatively lower energy (around 0.5 kcal/mol) than the latter. These two configurations seem to be the same as the clusters that have been reported as the stable structure in the gas phase by Rosas-Garcia et al.[19]. The ADDF method can further explore less stable structures, such as Structures **11** and **12**.

The substitution of a Mg ion for Ca in a trimer, $Ca_2Mg(CO_3)_3$, changes the cluster structure (Fig. 5). In most of the

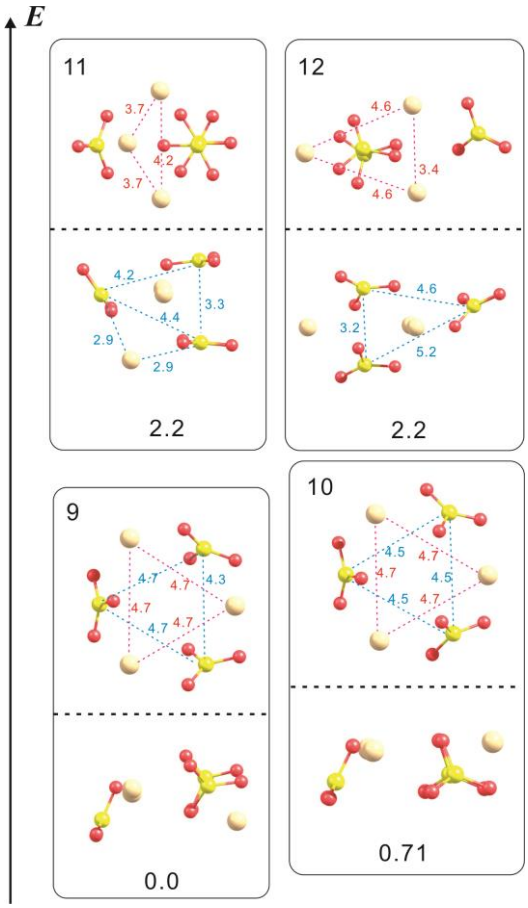

Fig. 4. Typical equilibrium structures of additive-free calcium carbonate trimers $(CaCO_3)_3$. In this system, Structure **9** is the most stable. Dotted lines and their supscripts represent the interatomic distance in Å.

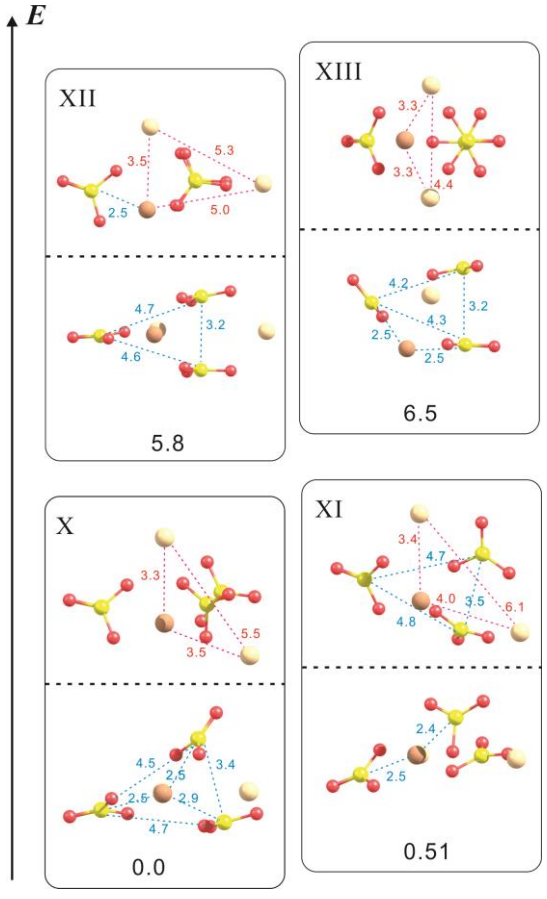

Fig. 5. Typical equilibrium structures of Mg-containing trimers, $Ca_2Mg(CO_3)_3$. Dotted lines and their supscripts represent the interatomic distance in Å.

arrangements of clusters with low energy (Structures **X** and **XI**), the Mg ion is located at the centre of the cluster and all three CO_3 ions are arranged around the Mg ion, which is the same tendency as with dimers. However, in the case of a pure $CaCO_3$ trimer, the CO_3 groups are uniformly distributed in the cluster with no ions in the centre (Structures **9** and **10**). As a result, the symmetry of the Mg-containing cluster becomes lower than that of a pure $CaCO_3$ trimer. Structures similar to the configuration appearing in the pure $CaCO_3$ trimer (Structures **11** and **12**) can be found as Equilibrium Structures **XIII** and **XII**, respectively, but these structures are much less stable than those of the pure $CaCO_3$ case. Furthermore, it is noted that, in both pure and Mg-containing cases, the most stable trimer structure (Structures **9** and **X**) is easily achieved from the most stable dimer structure (Structures **1** and **I**) by attaching one $CaCO_3$ ion pair.

3.2 Onset of the anhydrous crystalline phase

As shown from the previous experimental results, ACC easily forms from supersaturated solutions[35]; therefore, we can expect that the formation of a structure similar to that of the crystalline phase requires a large number of $CaCO_3$ units. However, surprisingly, the structure most similar to the crystalline phase of $CaCO_3$ appears when only four $CaCO_3$ units aggregate into the cluster. The most stable structure for additive-free tetramers $(CaCO_3)_4$ (Fig. 6) is the one in which Ca ions are arranged as a trigonal pyramid and CO_3 ions are arranged as a reversed trigonal pyramid with each CO_3 ion parallel to the bottom planes of the Ca pyramid. The CO_3 ion located at the top of the CO_3 pyramid is aligned with the Ca ion at the top of the Ca pyramid along the direction perpendicular to the bottom planes of these pyramids. This arrangement of Ca and CO_3 ions is almost the same as the local setting of these ions in calcite structures, which is referred to as a 'cubic closed-packing structure of the NaCl type' (Figs. 8a and b). In this structure, the Ca layers show an ABCABC sequence along the *c* axis. Because the Ca layers are separated by CO_3 layers, which have two opposite orientations, the calcite stacking can be described as $AC_1BA_2CB_1AC_2BA_1CB_2$. This structural feature leads to the stacking sequence in which Ca ions are aligned by CO_3 groups, which can be observed in the tetramer with structure **13**. Previously, Roass-García et al. has reported that the structure of $(CaCO_3)_n$ clusters in gas phases is not similar to that of crystalline phases[19]; however, the structure appearing in the present study is obviously related to the structure of calcite. The present calculation's adoption of the solvent effect may account for these differences.

Further comparison between the stable structure of the tetramer obtained in the present study (Structure **13**) and the local arrangement of ions in the calcite structure (Fig. 8b) shows a 30° difference in the rotation angle of CO_3 although the positions of Ca and CO_3 ions are almost the same, including their interatomic distance. Furthermore, in the case of the additive-free tetramer, other structures with rotated or tilted CO_3 are found as the equilibrium structures with low energy differences. CO_3 rotational order-disorder has been reported in the calcite structure[37–40], and CO_3 groups are rotated with relatively low activation barriers. Therefore, clusters with structures where Ca and CO_3 are staked the same as in calcite structures would lead to calcite formation.

In contrast, the most stable structure of Mg-containing tetramers, $Ca_3Mg(CO_3)_4$, is definitely different from pure $CaCO_3$ tetramers. In Structure **XIV** (Fig. 7) Cations form a flat triangular pyramid and Mg locates the top of this pyramid. Three CO_3 groups locate between Ca ions and form a triangle, and another CO_3 group is located immediately above one of the CO_3 groups when viewed from a direction vertical to a Ca and CO_3 triangular surface. The arrangement of a CO_3 group located on another CO_3 group along the axis vertical to the CO_3 plane is a feature of the aragonite structure, which is related to a hexagonal-close

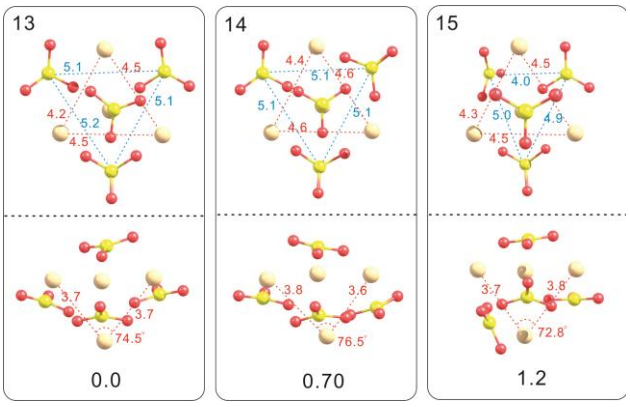

Fig. 6. Typical equilibrium structures of additive-free calcium carbonate tetramers $(CaCO_3)_4$. The most stable structure is **13**. Atomic distances between Ca ions are shown with red letters, and distances between CO_3 ions are with blue letters in Å. In this structure, the stacking manner of Ca and CO_3 is almost the same as that for calcite structure.

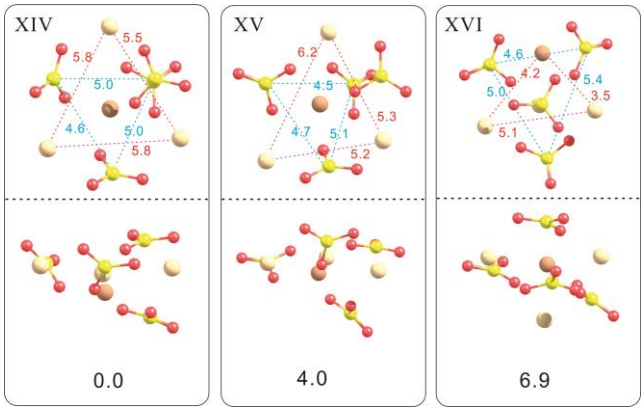

Fig. 7. Typical equilibrium structures of Mg-containing tetramers, $Ca_3Mg(CO_3)_4$. Atomic distances between Ca ions are shown with red letters, and distances between CO_3 ions are with blue letters in Å. The most stable structure is **XIV**, which resembles aragonite structure in its arrangement of CO_3 ions.

packing of the NiAs structure (Fig. 8c). In this structure, the Ca and CO_3 stacking is shown as $AC_1BC_2AC_1BC_2$; Ca atoms are aligned only with other Ca atoms along the *c* axis, and CO_3 groups are aligned only with other CO_3 groups. That is, in the stable structure of Mg-containing calcium carbonate tetramers, while the arrangement of cations is more flat than that in bulk aragonite structures, the stacking manner of CO_3 groups resembles the local arrangement of CO_3 in bulk aragonite, even though Mg-containing carbonate have a calcite structure and not an aragonite structure

ADDF also found another structure in which a Mg ion is not located at the centre of the cluster, which is similar to the configuration of additive-free $CaCO_3$ tetramers. However, this structure has higher energy and is less stable than that of additive-free tetramers. Furthermore, the most stable structure of Mg-containing trimers (Structure **X**) is similar to the most stable structure of tetramers (Structure **XIV**), and it is easy to grow Mg-containing trimers into this tetramer by simply attaching a $CaCO_3$ ion pair without any significant changes of interatomic distances. These results indicate that aragonite-related structures would be easy to form when Mg is present, which suggests that incorporation of Mg may have something to do with aragonite formation.

3.3 Aggregation path of the $CaCO_3$ cluster

In this section, we discuss the aggregation process of $CaCO_3$ clusters. One possible way to analyse the aggregation process is to create the energy map of a tetramer, as we did in the case of the $CaCO_3$ dimer, and to search the possible processes in the potential surface. However, we conducted our investigation by comparing the stabilization energies of different clusters to be more easily understood. The stabilization energy per monomer can be expressed as follows[19]:

$$E_{\mathrm{stab}} = \frac{E_{\mathrm{cluster}} - \mathrm{n}E_{\mathrm{monomer}}}{\mathrm{n}} \quad (1)$$

where n is the amount of $CaCO_3$ and $MgCO_3$ units in the cluster. In Fig. 9, the stabilization energy for pure and Mg-containing $CaCO_3$ clusters is plotted against cluster size. That figure shows that pure $CaCO_3$ clusters stabilize as the number of $CaCO_3$-containing clusters increases. This tendency is consistent with previous studies[11,14,18]. Also in Mg-containing cases, larger clusters are more stable, and the clusters have more stabilization energy than do pure $CaCO_3$ clusters.

Regarding the aggregation route of clusters, the growth of these clusters occurs by the aggregation of $CaCO_3$ or $MgCO_3$ units—not by the attachment of ions, as previous MD calculations regarding $CaCO_3$ cluster growth suggest[14]. Here we calculated the total energy of the combinations of clusters in the system, including four $CaCO_3$ and one $MgCO_3$ ion pairs. When determining the energy of each cluster, the energy of the

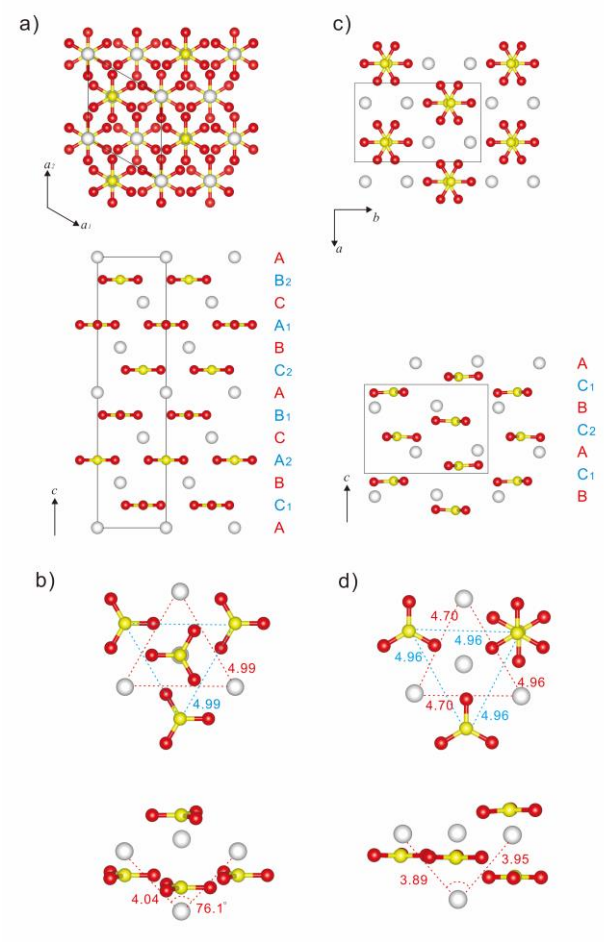

Fig. 8. (a) Bulk calcite structure, (b) local setting of Ca and CO_3 in a calcite structure, (c) bulk aragonite structure and (d) local setting of Ca and CO_3 in an aragonite structure. These figures were drawn with the VESTA program[36].

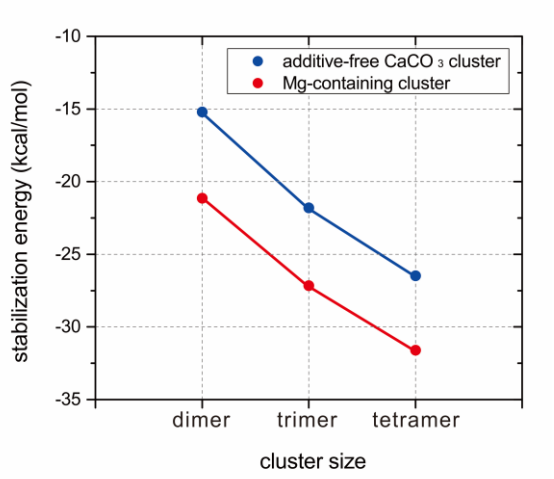

Fig. 9. Stabilization energy per monomer, varying with cluster size.

most stable structure was used. Fig. 10 shows how much energy decreases when clusters form where once only $CaCO_3$ and $MgCO_3$ ion pairs existed. This figure suggests that, in the most energetically favourable path, a Mg-containing dimer forms first and becomes larger by the attachment of a single $CaCO_3$ ion pair before other clusters form. This result is supported by the structural analysis discussed earlier, where the stable structures of Mg-containing trimers and teteramers are easily achieved from the stable arrangement of Mg-containing dimers and trimers simply by attaching one $CaCO_3$ unit.

As mentioned above, Mg forms a tight hydration shell with water molecules in aqueous solutions from which it is not easily released. However, the present calculation results indicate that once a Mg ion can be released from the hydration shell, it can be easily incorporated into clusters, which leads to aragonite formations. This tendency is consistent with experimental results, showing that aragonite tends to nucleate from aqueous solutions with a relatively high Mg content[3]. Furthermore, the present calculation may explain another experimental result:

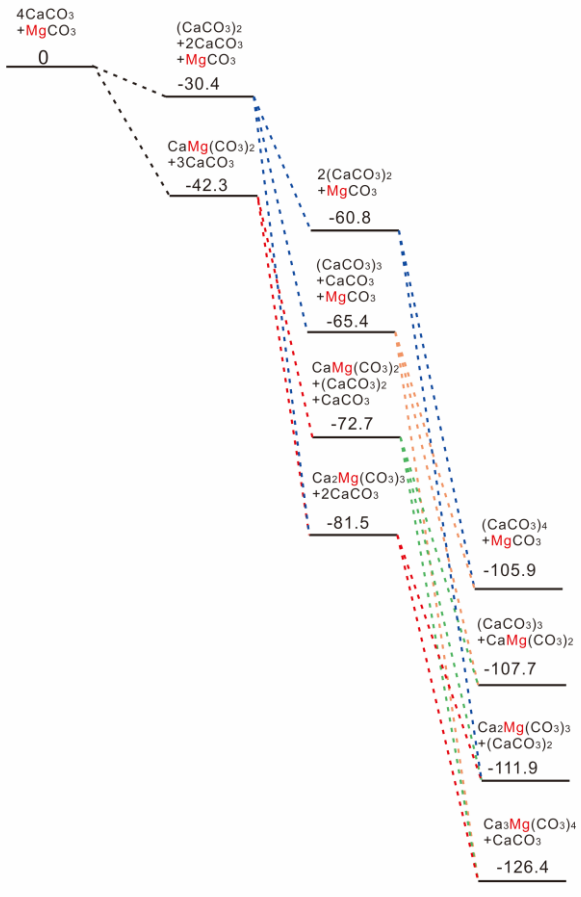

Fig. 10. Change of the system's total energy when four $CaCO_3$ and one $MgCO_3$ units are included during the aggregation process. Relative energies, compared with the condition in which only $CaCO_3$ and $MgCO_3$ ion pairs exist, are also shown in kcal/mol.

aragonite is easier to form at a relatively high temperature[6]. Under this condition, Mg can be easily released from hydration shells[41]; therefore, only a small amount of Mg^{2+} may lead to the formation of aragonite at high temperature. The present calculations provide the possibility that Mg can play a key role in aragonite formation not only by inhibiting calcite growth but also by directly promoting aragonite nucleation during early-stage $CaCO_3$ formation.

These results show that ADDF, even at this stage, is highly useful for analysing the atomic behaviour of the formation of small $CaCO_3$ clusters. However, of course, especially in the case for Mg-containing $CaCO_3$, larger clusters should be investigated in order to clarify the relationship between the cluster and crystalline polymorph forming after that. It is not only because the most stable structure of Mg-containing tetramer is not exactly same as the local setting of bulk structure but because it is not sure that small aragonite-like clusters continue to actual aragonite structure. For further extensions of the present work to the larger clusters, we need to consider some strategies. For example, use of the artificial force induced reaction (AFIR) algorithm[42], which was recently implemented in a developmental version of the GRRM program, would allow for applications to the larger clusters. Use of large scale computational resources would also expand its applicability. The more promising way is to adopt a semi-empirical theory or an empirical force-field in PES calculations. In this study, we directly explored the PES of the density functional theory adopting a hybrid functional and localized basis sets. This approach is expensive, though expected to provide a reliable set of geometries. Thus, in addition to the scientific finding concerning the very initial stage of the crystal growth, the present hybrid-DFT results for small clusters would be a good reference for future semi-empirical or empirical studies. Applications of the GRRM program to larger clusters taking these strategies are future subjects. Particularly, we are interested in the enlargement process of $CaCO_3$ cluster including up to 20 $CaCO_3$ unit, which may be more directly related to the structure of crystalline phase forming after these clusters[43]. The other phenomena such as the interaction between organic molecules and $CaCO_3$[44], and the formation of other materials such as phosphate or biphosphate[45,46], will also be interesting future subjects.

4. Conclusions

In order to clarify the effect of Mg^{2+} on the nucleation of calcium carbonate polymorphs, the stable structures of anhydrous additive-free and Mg-containing calcium carbonate clusters are derived using the anharmonic downward distortion following (ADDF) method. Optimization was performed at the B3LYP/6-31+G(d) level and the solvent effect was induced by the self-consistent reaction force method with the polarizable conductor calculation model. Calculation results show that incorporation of Mg^{2+} into clusters can change stable configurations as follows.

(1) In the case of dimers and trimers, a Mg ion strongly prefers to locate at the centre of the clusters.
(2) The crystalline phase appears when only four $CaCO_3$ units aggregate into the cluster: in the stable structure of additive-free $CaCO_3$ tetramers, arrangement of the Ca and CO_3 ions is almost the same as that for calcite structures; Mg-containing $CaCO_3$ tetramers resemble aragonite structures in the stacking manner of CO_3 ions.
(3) In the most energetically favourable path for the growth of clusters, a Mg-containing dimer forms first and becomes larger by the attachment of a single $CaCO_3$ ion pair before other clusters form.

These results suggest that Mg is easy to incorporate into the clusters once it is released from its tight hydration shell and that Mg can play a key role in aragonite formation during early-stage $CaCO_3$ formation.

These results also indicate that the ADDF method is highly useful for the investigation of atomic behaviour during early-stage $CaCO_3$ formation. Further exploration of stable and transition structures in larger system, including water and bicarbonate molecules, should provide the new insights in this field.

Acknowledgements

The authors thank H. Sakuma and K. Nakamura for their discussion and useful comments. The authors would also like to thank the anonymous reviewers for their constructive comments. This work was supported by JSPS KAKENHI Grant Numbers 26870010, 15H05731.

Notes and references

1 S. Weiner and P. M. Dove, *Rev. Mineral. Geochem*, 2003, **54**, 1.
2 J. Johnston, H. E. Merwin and E. D. Williamson, *Am. J. Sci.*, 1916, **4**, 473.
3 Y. Kitano, *Bull Chem Soc Japan*, 1962, **35**, 1973.
4 O. Shönel and J. W. Mullin, *J. Cryst. Growth*, 1982, **60**, 239.
5 T. Ogino, T. Suzuki and K. Sawada, *Geochim Cosmochim Acta*, 1987, **51**, 2757.
6 J. Kawano, A. Miyake, N. Shimobayashi and M. Kitamura, *J. Phys: Condens. Matter*, 2009, **21**, 425012.
7 L. C. Nielsen, J. J. De Yoreo and D. J. DePaolo, *Geochim Cosmochim Acta*, 2013, **115**, 100.
8 K. J. Davis, P.M. Dove and J.J. De Yoreo, *Science*, 2000, **290**, 1134.
9 D. Gebauer, A. Völkel and H. Cölfen, *Science*, 2008, **322**, 1819.
10 D. Geabuer and H. Cölfen, *Nano Today*, 2011, **6**, 564.
11 D. Gebauer, M. Kellermeier, J. D. Gale, L. Bergström and H. Cölfen, *Chem. Soc. Rev*., 2014, **43**, 2348.
12 A. F. Wallace, L. O.Hedges, A. Fernandez-Martinez, P. Raiteri, J. D. Gale, G. A. Waychunas, S.Whitelam, J. F. Banfield and J. J. De Yoreo. *Science*, 2013, **341**, 885.
13 E. M. Pouget, P. H. H. Bomans, J. A. C. M. Goos, P. M. Frederik, G. de With and N. A. J. M. Sommerdijk, *Science*, 2009, **323**, 1455.
14 G. A. Tribello, F. Bruneval, C. C. Liew and M. Parrinello, *J. Phys. Chem. B*, 2009, **113**, 11680.
15 P. Raiteri and J. D. Gale, J. Am. Chem. Soc., 2010, 132, 17623.
16 D. Quigley and P. M. Rodger, *J. Chem, Phys.*, 2008, **128**, 221101.
17 D. Quigley, C. L. Freeman, J. H. Harding and P. M. Rodger, *J. Chem, Phys.*, 2011, **134**, 044703.
18 R. Demichelis, P. Raiteri, J.D. Gale, D. Quigley and D. Gebauer, *Nat. Commun.*, 2011, **2**, 590.
19 V. M. Rosas-García, I.C. Sáenz-Tavera and D.E. Cantú-Morales, *J. Clust. Sci.*, 2012, **23**, 203.
20 J. Kawano, H. Sakuma and T. Nagai, *Prog. Earth Planet. Sci.*, 2015, **2:7**, doi:10.1186/s40645-015-0039-4.
21 K. Ohno and S. Maeda, *Chem. Phys. Lett.*, 2004, **384**, 277.
22 S. Maeda and K. Ohno, *J. Phys. Chem. A*, 2005, **109**, 5742.
23 K. Ohno and S. Maeda, *J. Phys. Chem*. *A*, 2006, **110**, 8933.
24 S. Maeda, T. Taketsugu, K. Morokuma and K. Ohno, *Bull. Chem. Soc. Jpn.*, 2014, **87**, 1315.
25 M. Elango, G. S. Maciel, F. Palazzetti, A. Lombardi and V. Aquilanti. *J. Phys. Chem. A,* 2010, **114**, 9864.
26 S. Ohno, K. Shudo, M. Tanaka, S. Maeda and K. Ohno, *J. Phys. Chem C*, 2010, **114**, 15671.
27 K. Omori, H. Nakayama and K. Ishii, *Chem. Lett.*, 2014, **43**, 1803.
28 G. Kaur and Vikas, *J. Phys. Chem. A*, 2014, **118**, 4019.
29 S. Miertus, E. Scrocco and J. Tomasi, *Chem. Phys.* 1981, **55**, 117.
30 M. J. Frisch, et al., Gaussian09, Gaussian Inc., Wallingford, CT 06492, USA.
31 S. Maeda and K. Ohno, *J. Phys Chem. A*, 2007, **111**, 4527.
32 V. Barone and M. Cossi, *J. Phys. Chem. A*, 1998, **102**, 1995.
33 S. Md. Pratik, S. Chakraborty, S. Mandal and A. Datta, *J. Phys, Chem. C*, 2015, **119**, 926.
34 S. Md. Pratik and A. Datta, *J. Phys, Chem. C*, 2015, **119**, 15770.
35 J. H. Cartwright, A. G. Checa, J. D. Gale, D. Gebauer and C. I. Sainz-Diaz, *Angew. Chem. Int. Ed.* 2012, **51**, 11960.
36 K. Momma and F. Izumi. *J Appl Crystallogr*, 2009, **41**, 653.
37 S. A. Redfern, E. Salje and A. Navrotsky, *Contrib. Mineral. Petrol.*, 1989, **101**, 479.
38 M. J. Harris, *Am. Mineral.*, 1999, **84**, 1632.
39 M. T. Dove, I. P. Swainson, B. M. Powell and D. C. Tennant, *Phys. Chem. Minerals*, 2005, **32**, 493.
40 J. Kawano, A. Miyake, N. Shimobayashi and M. Kitamura, *J. Phys: Condens. Matter*, 2009, **21**, 095406.
41 P. Zhang, M. T. Tweheyo and T. Austad, *Colloid. Surface. A*, 2007, **301**, 199.
42 S. Maeda, T. Taketsugu, K. Morokuma, *J. Comput. Chem.*, 2014, **35**, 166.
43 A. M. Bano, P. M. Rodger, and D. Quigley, *Langmuir*, 2014, **30**, 7513.
44 T. Lee and J. G. Chen, *Cryst. Growth and Des.*, 2009, **9**, 3737.
45 T. Lee and Y. C. Lin, *Cryst. Growth and Des.*, 2011, **11**, 2973.
46 W. J. Habraken, J. Tao, L. J. Brylka, H. Friedrich, L. Bertinetti, A. S. Schenk, A. Verch, V. Dmitrovic, P. H. Bomans, P. M. Frederik, J. Laven, P. van der Schoot, B. Aichmayer, G. de With, J. J. DeYoreo, and N. A. Sommerdijk, *Nat. Comm*., 2013, **4**, 1507.